# Ultrasonic Contrast Agent Shell Rupture Detected by Inertial Cavitation and Rebound Signals

Azzdine Y. Ammi, Robin O. Cleveland, Jonathan Mamou, *Member, IEEE*, Grace I. Wang, S. Lori Bridal, *Member, IEEE*, and William D. O'Brien, Jr., *Fellow, IEEE*

***Abstract*—Determining the rupture pressure threshold of ultrasound contrast agent microbubbles has significant applications for contrast imaging, development of therapeutic agents, and evaluation of potential bioeffects. Using a passive cavitation detector, this work evaluates rupture based on acoustic emissions from single, encapsulated, gas-filled microbubbles. Sinusoidal ultrasound pulses were transmitted into weak solutions of Optison$^{TM}$ at different center frequencies (0.9, 2.8, and 4.6 MHz), pulse durations (three, five, and seven cycles of the center frequencies), and peak rarefactional pressures (0.07 to 5.39 MPa). Pulse repetition frequency was 10 Hz. Signals detected with a 13-MHz, center-frequency transducer revealed postexcitation acoustic emissions (between 1 and 5 $\mu$s after excitation) with broadband spectral content. The observed acoustic emissions were consistent with the acoustic signature that would be anticipated from inertial collapse followed by "rebounds" when a microbubble ruptures and thus generates daughter/free bubbles that grow and collapse. The peak rarefactional pressure threshold for detection of these emissions increased with frequency (e.g., 0.53, 0.87, and 0.99 MPa for 0.9, 2.8, and 4.6 MHz, respectively; five-cycle pulse duration) and decreased with pulse duration. The emissions identified in this work were separated from the excitation in time and spectral content, and provide a novel determination of microbubble shell rupture.**

## I. Introduction

Ultrasonic contrast agents (UCAs) consist of small, stabilized microbubbles (diameter $< 10$ $\mu$m) that are injected intravenously to enhance contrast of ultrasonic images and enable nonlinear imaging capabilities. Enhanced sonographic contrast improves early detection of a large variety of disease processes [1], [2]. Novel imaging techniques have been developed using the nonlinear UCA response to detect blood flow in tissue parenchyma. By provoking local acoustic destruction in a selected region in situ to purposefully modify contrast concentration, dynamic evaluation of image contrast-enhancement can be used to assess blood volume and flow rate [3], [4]. However, UCA-based blood perfusion assessment is hampered by unintentional modification of UCA concentration during imaging and the unknown ultrasound backscattered echo contribution to the received signal by microbubble destruction. If the origin of the desired image enhancement is linked to the destruction of the microbubbles, the transmit parameters should be set above the destruction threshold. On the contrary, if the image's goal is to follow intact UCAs, the transmit settings need to minimize or eliminate UCA destruction. Thus, knowledge of the UCA destruction thresholds is essential for many innovative but sensitive imaging techniques. An understanding of microbubble destruction is also fundamental for development of targeted contrast microbubbles carrying encapsulated medicines to a site for delivery initiated by ultrasonic capsule destruction [5], [6].

A strong experimental basis is needed to guide theoretical model developments [7]–[9] so that modifications of bubble dynamics described by these models can be applied to predict destruction thresholds based on UCA properties (e.g., composition of encapsulating shell, gas, size distribution). The need to respond to such practical concerns and the potential to develop new UCA applications have generated considerable interest in the elucidation and quantification of UCA destruction thresholds [10]–[13]. Several techniques have been used. The passive cavitation detector (PCD) technique uses a receiver to listen passively for acoustic emissions from bubbles excited by another source [14], [15]. Giesecke and Hynynen [10] used a PCD to determine the cavitation thresholds based on the peak rarefactional pressure amplitude that caused an increase in the broadband noise emission. This increase was empirically chosen to be greater than one standard deviation above the baseline noise. As determined by this method, the inertial cavitation (IC) thresholds of Optison$^{TM}$ [Amersham Health (GE Healthcare), Princeton, NJ] increased with frequency (approximately 0.1 MPa at 0.74 MHz, 0.2 MPa at 1.1 MHz, 0.4 MPa at 2.18 MHz, and 1.6 MPa at 3.3 MHz). This study, which used long

Manuscript received December 29, 2004; accepted June 16, 2005. This work was supported by NIH Grant EB02641 (formerly HL58218) awarded to the University of Illinois at Urbana-Champaign.

A. Y. Ammi and S. L. Bridal are with the Laboratoire d'Imagerie Paramétrique, UMR 7623 C.N.R.S., 75006 Paris, France (e-mail: bridal@lip.bhdc.jussieu.fr).

R. O. Cleveland is with the Department of Aerospace and Mechanical Engineering, Boston University, Boston, MA 02215.

J. Mamou was with the Bioacoustics Research Laboratory, Department of Electrical and Computer Engineering, University of Illinois at Urbana-Champaign, Urbana, IL 61801. He is now with the Frederic L. Lizzi Center for Biomedical Engineering, Riverside Research Institute, New York, NY.

G. I. Wang and W. D. O'Brien, Jr. are with the Bioacoustics Research Laboratory, Department of Electrical and Computer Engineering, University of Illinois at Urbana-Champaign, Urbana, IL 61801.

incident pulses (from 2 to 100 ms), found that pressure thresholds did not vary strongly as a function of pulse duration (PD). Chen *et al.* [11] also used a PCD to estimate fragmentation pressure thresholds for four contrast agents (at 1.1 and 3.5 MHz). They selected the fragmentation threshold to correspond to the incident peak rarefactional pressure simultaneously satisfying two criteria. The first criterion was that 5% of "spikes" in the received signal exceeded a voltage threshold. The second criterion was that the signal's spectral amplitude increased between harmonics (broadband noise). The acoustic fragmentation thresholds of three UCAs [Optison™, Sonazoid (Nycomed Amersham, Oslo, Norway), and biSphere (Point Biomedical, San Carlos, CA)] were estimated for various acoustic exposure conditions. Optison™ had mean fragmentation pressure thresholds of 0.13 MPa at 1.1 MHz and 0.48 MPa at 3.5 MHz. A PD of at least five cycles was necessary for Optison™ microbubbles to achieve steady-state fragmentation thresholds. Comparison of threshold levels reported for Optison™ under similar conditions [10], [11] revealed that the levels may vary, depending on criteria applied to signals received during microbubble excitation.

Active cavitation detection (ACD) also has been used to estimate UCA collapse thresholds in which the receiver interrogates the region of interest with a low-pressure pulse amplitude in order to assess the potential cavitation effects from another ultrasound exposure of that same region [16]–[18]. Chen *et al.* [19] used an ACD to study the dependence of ultrasound-induced IC on the PD. The dependence of IC activity and hemolysis generated by 1.15-MHz ultrasound as a function of PD (between 5 and 200 cycles) was conducted using a constant rarefractional pressure (3 MPa) and constant energy. Two UCAs were used [Optison™ and Albunex® (MBI, San Diego, CA)]. With Optison™, only 2 of 10 tests under the 50-cycle PD condition generated detectable microbubble signals. For the longer PDs (e.g., 100 and 200 cycles), 9 of 10 tests showed variable amounts of generated microbubbles. Hence, more microbubbles were generated under longer PD conditions. Using Optison™, up to 60% hemolysis was produced with the longer PDs (100 and 200 cycles), compared with $<10\%$ hemolysis with the shorter PDs (5 and 10 cycles). Albunex® generated considerably less IC activity and hemolysis than that produced using Optison™.

Acoustic attenuation modifications also have been used to evaluate UCA destruction. Chang *et al.* [16] defined the threshold as the peak rarefactional pressure that caused total destruction of UCAs in a suspension when exposed to high intensity focused ultrasound (HIFU) at 1.1 MHz. The total destruction of UCAs was determined when the echo amplitude from the rear wall of a tube filled with UCA returned to the amplitude observed prior to the introduction of UCA in the suspension. Their results showed that the total destruction pressure threshold increased with increasing Albunex® concentration and decreased with increasing pulse repetition frequency (PRF). This threshold decreased with increasing the PD in terms of the number of cycles $N$ for $N < 10$ and was independent of the number of cycles for $N > 10$. However, because the return to baseline criterion detects total destruction of all UCA in a solution, onset of microbubble destruction cannot be assessed by this technique, nor does it permit isolation of the response from a single microbubble.

Optical observation also has been used to investigate UCA response. Chomas *et al.* [12] used a high-speed camera to experimentally observe the destruction of isolated UCA microbubbles. Within the studied frequency range, fragmentation threshold of the experimental agent studied was shown to decrease with increasing pressure and increase with frequency (resonance frequency not reported). This direct optical observation approach is currently the reference for measuring UCA fragmentation thresholds, but the expensive equipment necessary for its application limits the technique's accessibility and is not usable for in vivo studies of optically opaque human organs.

We report on a technique that uses passive cavitation detection. However, instead of analyzing signals received during acoustic excitation, broadband emissions occurring between 1 and 5 $\mu$s after excitation were identified. We have linked these signals to the inertial cavitation (sometimes followed by rebounds) of bubbles released after UCA shell rupture, and refer to the minimum incident peak rarefactional pressure leading to such an event as the minimum rupture threshold. Because these emissions were separated in time and spectral content from the main echo, they were easily distinguished from the principal microbubble response (e.g., oscillations and shell rupture). Thus, the detection of shell rupture thresholds using IC emissions as proposed herein is different from previously reported approaches using passive cavitation detection and has several potential advantages over other techniques described in the literature. Detecting UCA rupture from signals during the acoustic excitation is confounded by the presence of spectral components from many sources, for example, nonlinear propagation of the incident pressure pulse and nonlinear microbubble dynamics. The inertial collapse and rebound signals are not contaminated by nonlinear spectral content from other sources. Thus, detection of these postexcitation signals provides a more robust detector of UCA rupture than can be obtained through analysis of the principal response.

Second, and this is true for all PCD-based techniques, the equipment necessary to make the measurements is less complex and expensive than that required for a high-speed camera, and the PCD has the potential to detect the rupture thresholds in vivo as has been done in lithotripsy [20].

Third, the literature related to UCA destruction applies a variety of terms to describe destruction thresholds such as fragmentation, cavitation, rupture, and collapse. In effect, each term refers to specific aspects of the destruction process [21], [22]. By comparing our experimental results with numerical simulations of the dynamics of shelled microbubbles, we find that our observations are consistent with the inertial cavitation response of a free bubble that is released after the rupture of the shell of a UCA.

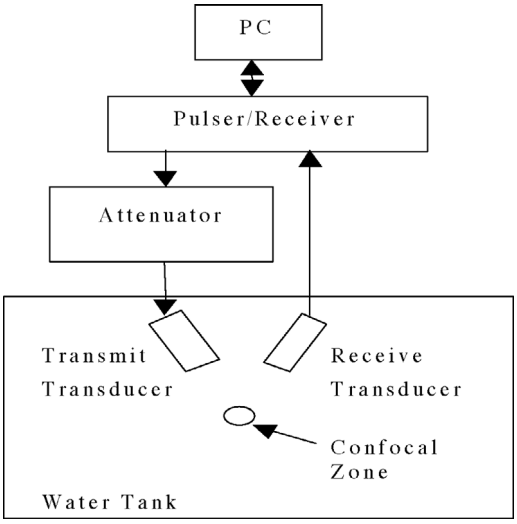


Fig. 1. Experimental configuration of the passive cavitation detector.

## II. Materials and Methods

### A. Contrast Agent

Experiments were conducted using Optison™ an FDA-approved UCA. These microbubbles have an albumin shell, approximately 15-nm thick, encapsulating perflutren $C_3F_8$ gas. The solution in the manufacturer's vial has a concentration between 5 and $8 \times 10^8$ microbubbles/mL. Approximately 93% of the microbubble diameters are less than 10 $\mu$m, with a maximum diameter of 32 $\mu$m and a mean diameter in the range of 2–4.5 $\mu$m [23].

### B. Ultrasound Exposure Setup and Pulse Waveforms

The experiments were carried out in a clear plastic tank (50.5-cm long × 25.5-cm wide × 30.0-cm high) containing $9.6 \pm 0.3$ L of degassed water (boiled, sealed, then cooled) between 20 and 22°C. Three 19.1-mm-diameter, single-element, focused (f/2) transducers (measured center frequencies of 0.9, 2.8, or 4.6 MHz) were used to insonify the microbubbles. Sinusoidal tone bursts were generated by a pulser-receiver (Ritec Advanced Measurement System RAM5000, Warwick, RI) for a selected combination of frequency (0.9, 2.8, or 4.6 MHz) and PD (three, five, or seven cycles). At 0.9 MHz, the measured PDs (determined from −6 dB of peak rarefactional pressure) were 5.8, 8.0, and 11.1 $\mu$s; at 2.8 MHz they were 1.5, 2.6, and 3.3 $\mu$s; and at 4.6 MHz they were 0.9, 1.4, and 2.0 $\mu$s for PDs of three, five, and seven cycles, respectively. Pulse phase was 0° (that is, the pulses lead with a phase of positive voltage) and PRF was 10 Hz for all experiments. The transmit pressure amplitude was varied using the pulser-receiver's output control settings. To fine tune (obtain smaller changes) the transmit pressure amplitude, a step-variable attenuation (Model 358, Arenberg Ultrasonic Laboratory, Boston, MA) was used (Fig. 1).

The transmit pressure waveforms were calibrated at the field's focus for each amplitude, frequency, and PD combination. Calibrations were performed according to well-established calibration techniques [24], [25] using a PVDF bilaminar shielded membrane hydrophone (diameter of the active element, 0.5 mm, Marconi 699/1/00001/100; GEC Marconi Ltd., Great Baddow UK).

TABLE I
Peak Rarefactional Pressures (MPa) of Incident Pressure Waveforms for Lowest and Highest Pulser/Receiver Settings.

| Cycles | 0.9 MHz | 2.8 MHz | 4.6 MHz |
|---|---|---|---|
| Three | 0.07–1.30 | 0.39–3.83 | 0.28–4.85 |
| Five | 0.09–1.52 | 0.48–4.13 | 0.32–5.40 |
| Seven | 0.10–1.60 | 0.51–4.31 | 0.35–5.39 |

Fig. 2(a) shows the hydrophone-measured waveform (at the focus) of the 4.6-MHz transducer for a seven-cycle PD at the lowest excitation level. The waveform was symmetric with peak rarefactional pressure and peak compressional pressure of 0.35 MPa. The temporal waveform was gated with a 10-$\mu$s Blackman window, zero padded to 8192 points, and an fast Fourier transform (FFT) was performed to determine frequency content [Fig. 2(b)]. The principal frequency component was observed at 4.6 MHz, corresponding to the measured transducer center frequency. A small harmonic component was observed at 9.2 MHz.

At the highest output setting for the 4.6-MHz transducer, the seven-cycle PD hydrophone-measured waveform (at the focus) is displayed in Fig. 3(a). The waveform was highly asymmetric with a peak rarefactional pressure of 5.39 MPa and peak compressional pressure of 11.9 MPa. This sort of asymmetry is characteristic of a diffracted beam that has undergone nonlinear propagation distortion [26]. Fig. 3(b) shows the corresponding spectrum in which the nonlinear propagation distortion manifests itself as the transfer of the energy from the fundamental (4.6 MHz) to the higher harmonics. This behavior demonstrates that harmonic signals scattered by a microbubble may not be solely due to nonlinear microbubble dynamics but likely include harmonic components present in the insonating pulse.

By repeating hydrophone measurements for all combinations of frequency, PD and output setting, the incident waveforms were calibrated over the peak rarefactional pressure range between 0.07 and 5.39 MPa (Table I). The maximum pressure difference measured between consecutive output settings was 0.5 MPa, and the minimum pressure change obtained using external attenuation was 0.05 kPa.

### C. Passive Cavitation Detector

A 13-MHz measured center-frequency focused transducer (12.7-mm diameter and 15.4-mm focal length), mounted confocal and at a 60° angle to the transmit beam axis, was used to passively collect emissions from the bub-

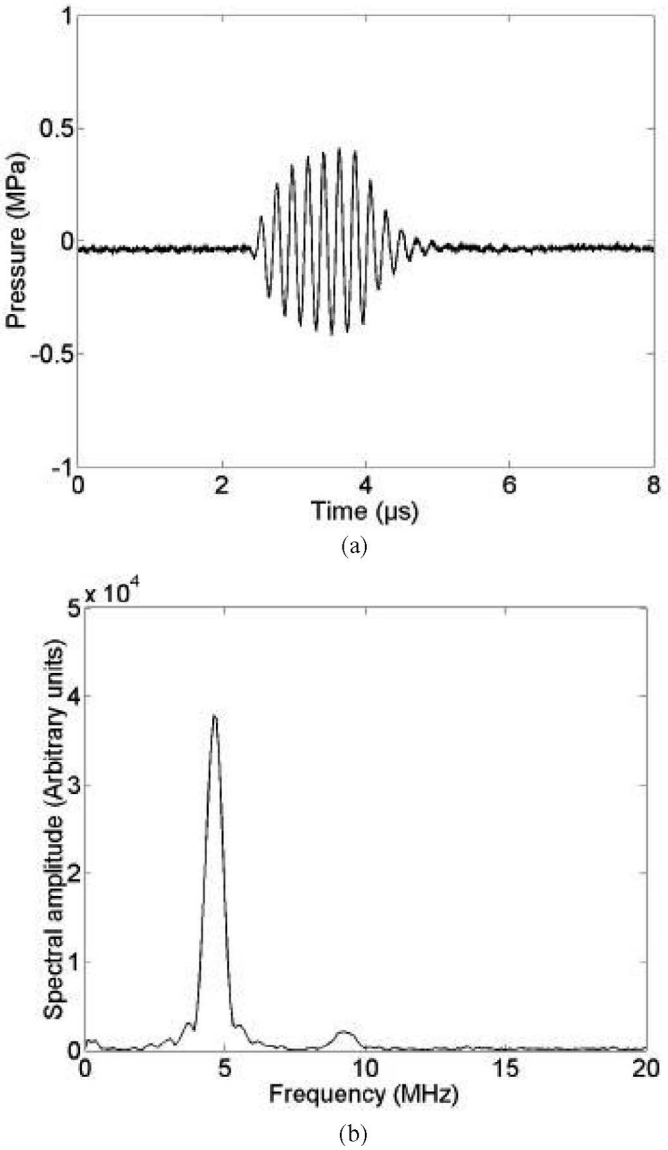


Fig. 2. Lowest amplitude excitation 4.6 MHz, seven-cycle waveform. (a) Pressure waveform measured at the transducer focus. (b) Corresponding amplitude spectrum.

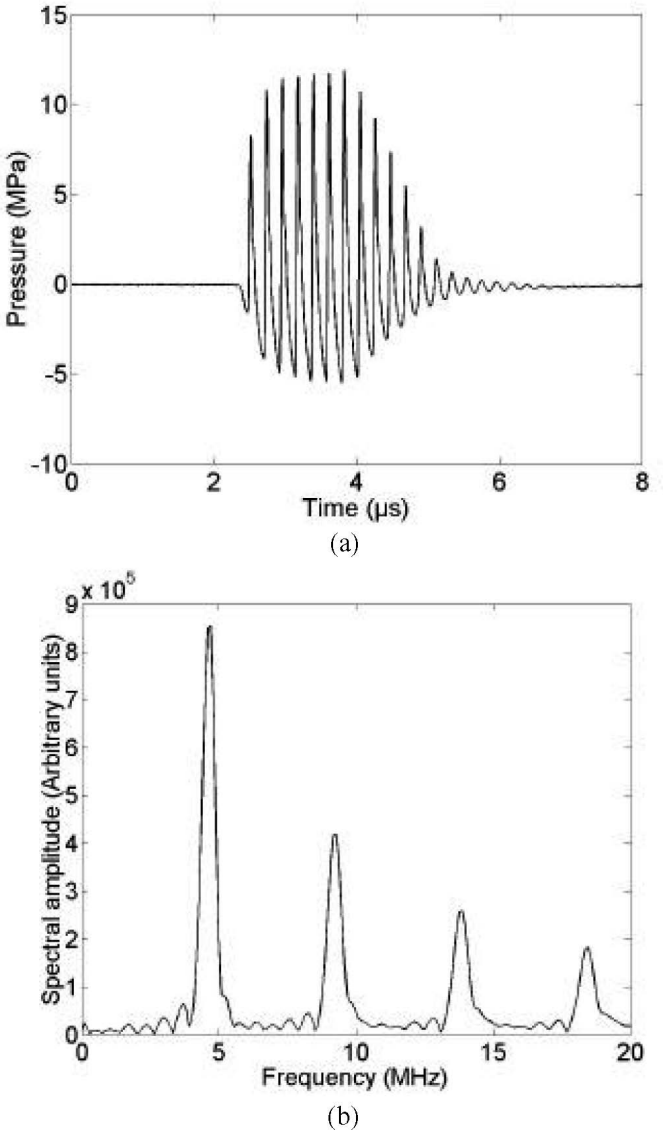


Fig. 3. Highest amplitude excitation 4.6 MHz, seven-cycle waveform. (a) Pressure waveform measured at the transducer focus. (b) Corresponding amplitude spectrum.

bles (Fig. 1). The −6 dB field limits were determined for each transducer by measuring the scattered signal from a 50-$\mu$m diameter wire reflector translated throughout the focal region in a pulse-echo configuration [27]. The characteristics of the four transducers are summarized in Table II.

The receiver's −6 dB field limits were fully inside those of the transmit transducers. Thus, the effective confocal volume corresponded to the 13-MHz transducer's −6 dB field limits: a cigar-shaped volume 3.38-mm long and 0.25 mm in diameter (approximate volume of 0.12 mm$^3$). The PCD passively detected signals from this volume and was primarily sensitive to frequencies greater than the transmit frequency range. The output from the receive transducer was amplified (44 dB), digitized (12-bit, 200 MHz, Strategic Test digitizing board UF 3025, Cambridge, MA) and saved to a personal computer. The data were processed off-line using Matlab® (The MathWorks, Inc., Natick, MA).

### *D. Data Acquisition*

The measurement protocol was as follows. The tank was filled with degassed water. The selected transmit transducer was aligned with the PCD receiver. A baseline data acquisition was made in the absence of contrast agent by acquiring 128 received waveforms at each transmit pressure amplitude. Using a graduated syringe, 0.2 mL of Optison$^{TM}$ was injected into the tank corresponding to approximately $10^8$ microbubbles, and resulted in a mean concentration in the tank of about 10 microbubbles/$\mu$L. Thus, on average, only 1 microbubble should be within the −6 dB receiver volume. The water was gently stirred with a pump before and during data acquisition to maintain an even distribution of the UCA in the water and to en-

TABLE II
MEASURED TRANSDUCER FIELD CHARACTERISTICS.

| Center frequency (MHz) | −6 dB bandwidth (MHz) | −6 dB beamwidth at focus (mm) |
|---|---|---|
| 0.9 | 0.8–1.0 | 3.0 |
| 2.8 | 2.6–3.0 | 2.3 |
| 4.6 | 4.3–4.8 | 1.9 |
| 13 | 9.3–17.6 | 0.2 |

sure its replenishment in the active volume. A three-cycle PD at the transducer center frequency was generated. For each transmit pressure amplitude (varied from highest to lowest), 128 consecutive received waveforms were acquired. This acquisition procedure was repeated for five-cycle PDs then seven-cycle PDs. Samples of a degassed water and Optison$^{TM}$ solution under the same conditions and at the same concentration as used for the experiments were observed under a microscope. Microbubbles were observed to remain intact throughout the experimental duration.

### *E. Data Analysis*

The direct current (DC) component of each received waveform was set to zero by subtracting its mean value. The noise level was evaluated from each baseline acquisition made in the absence of Optison$^{TM}$. Each set of waveforms acquired with Optison$^{TM}$ then was sorted from highest to lowest echo amplitudes. Then, each waveform was inspected and segments with signals above the noise level (indicating UCA response) were selected for further analysis. A sliding Blackman window (120 points, 0.6 $\mu$s) was moved along the selected portion of each zero-mean received waveform in steps of 0.025 $\mu$s. Windowed signals were zero padded to 8192 points, and their FFT was calculated (frequency resolution of 24 kHz). The frequency content of signals received from a microbubble in the interrogation volume during and after insonification was evaluated graphically by plotting these spectra as a function of time (spectrogram).

## III. RESULTS

Fig. 4 shows a representative echo waveform and its time-frequency spectrogram for a single microbubble. The 4.6-MHz, seven-cycle PD transmit pressure waveform had a peak rarefactional pressure of 0.95 MPa. The echo waveform between approximately 2 and 3 $\mu$s corresponds to the PCD response of the microbubble due to the excitation. In the spectrogram, the band centered near 9.3 MHz contains harmonics that may have been generated both by nonlinear bubble dynamics and nonlinear propagation distortion of the pulse incident on the microbubble. The thin vertical lines (at discrete times across a large range of frequencies) demonstrate that broadband content appears periodically during the compression phases. After the end of the excitation, no acoustic emissions are detected in the time trace.

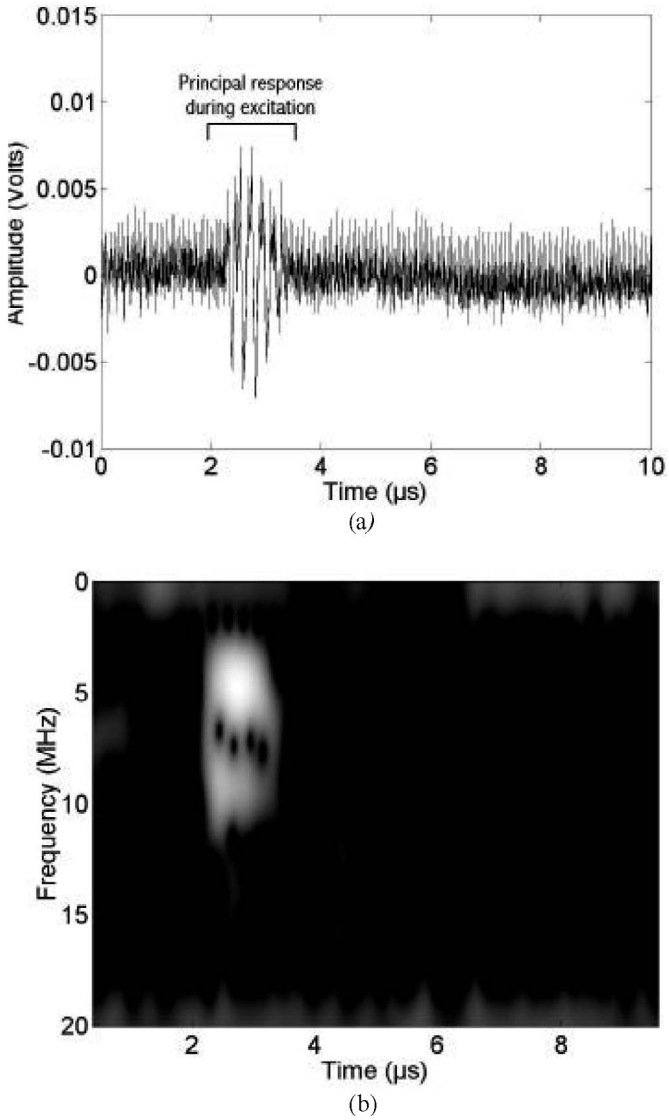


Fig. 4. PCD measurements (13-MHz receiver) for a 4.6-MHz, seven-cycle, 0.95-MPa peak rarefactional pressure excitation. (a) Time waveform. (b) Corresponding time-frequency spectrogram.

Fig. 5 shows an echo waveform and its time-frequency spectrogram for a single microbubble excited by 4.6-MHz, seven-cycle PD transmit pressure waveform with a peak rarefactional pressure of 2.82 MPa. The echo waveform between approximately 2 and 3 $\mu$s corresponds to the PCD response of the bubble due to the excitation. In the spectrogram, the strong bands near 10 and 15 MHz are harmonics generated both by nonlinear propagation distortion of the incident pulse and nonlinear bubble dynamics. The spectral amplitude near 9.3 MHz is approximately nine times higher in Fig. 5 than in Fig. 4. Again, thin vertical lines with broadband content appear periodically during the compression phases. After the end of the excitation, at about 4.5 $\mu$s (Fig. 5), a short-duration response is seen in the time trace, and a corresponding broadband signature (from 3 to 19 MHz) is observed in the spectrogram. Such

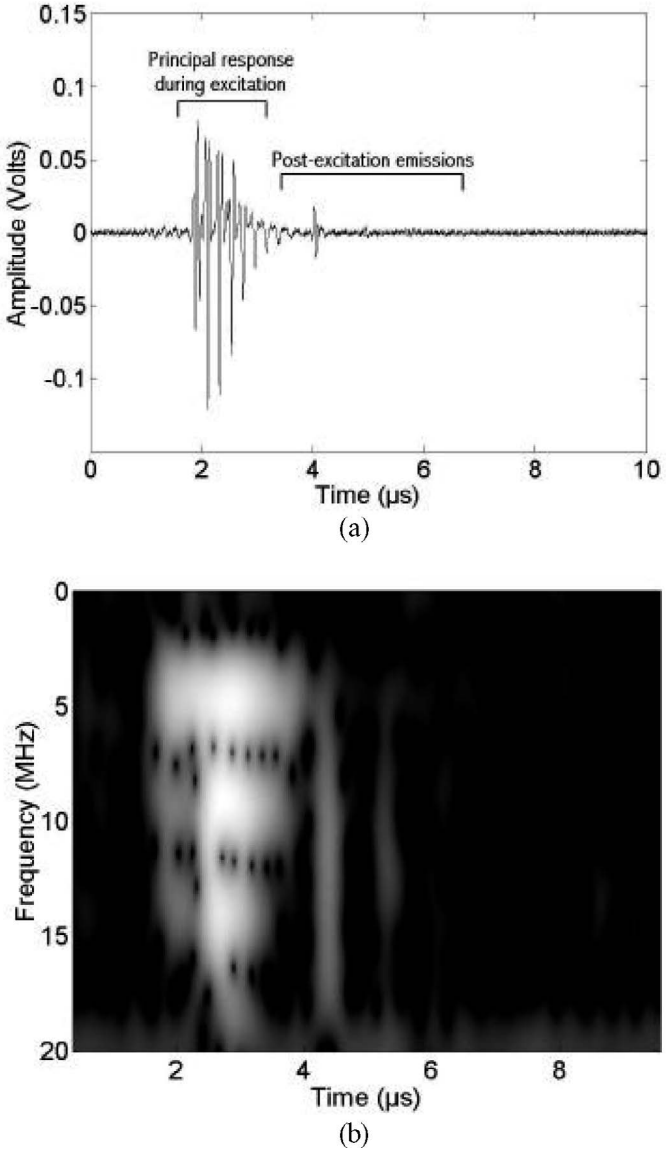


Fig. 5. PCD measurements (13-MHz receiver) for a 4.6-MHz, seven-cycle, 2.82-MPa excitation. (a) Time waveform. (b) Corresponding time-frequency spectrogram.

postexcitation, short-duration broadband response corresponds well to the anticipated acoustic signature due to the inertial collapse and "rebound" of daughter bubbles [21]. There also is evidence of a rebound at 5.5 $\mu$s. Such an event also is consistent with the existence of a free bubble undergoing inertial oscillations. The release of daughter bubbles following UCA shell rupture has been observed optically [13], [28]. After the shell has ruptured, unconstrained daughter bubbles are formed [21] that are able to grow and collapse essentially as free IC bubbles [29]. It is highly unlikely that the rebound signature could be generated by a microbubble that is still encapsulated because encapsulated microbubble oscillations are damped by the shell properties after the excitation. Thus we hypothesize that absence of postexcitation inertial collapse signals (Fig. 4) indicates that the shell has not ruptured. Therefore, we used the presence of the inertial collapse signal (followed in some cases by additional signals corresponding to rebounds) to define a minimum rupture threshold for the UCA, the lowest excitation peak rarefactional pressure for which an IC is detected from any of the acquired waveforms.

Fig. 6 shows the peak positive and peak negative voltages from the 13-MHz PCD receiver of the principal microbubble response as a function of the incident peak rarefactional pressure. Data are shown for three-, five- and seven-cycle PDs at 4.6-MHz transmit signal. Each point is the average value from the subset of the 128 acquired time traces in which a postexcitation, short-duration broadband response was detected. Error bars represent the standard deviation of this average.

For incident peak rarefactional pressures up to about 1.5 MPa (Fig. 6), there is a smooth and gradual increase in the peak voltage signals received during insonification. For incident peak rarefactional pressures greater than 1.5 MPa, there is a marked increase in the standard deviation of the 13-MHz PCD receive signals. This increase can be attributed to large variations in the pulse-to-pulse response of the microbubbles, presumably due to rupture of the contrast agents. The arrows in Fig. 6 indicate the incident peak rarefactional pressure thresholds at which the first (lowest incident peak rarefactional pressure) IC pulse was detected for each PD at 4.6 MHz. Inertial collapse and rebound signals were detected for peak rarefractional pressures at about 0.8 MPa. This is well below the onset of unsteady behavior of the peak PCD receive voltages. Thus, occurrence of IC and rebound signals appears to identify rupture at lower transmit pressures than would be identified based on modification of the voltage amplitude of the principal bubble response (percent of spikes in the principal microbubble response [11]).

The lowest incident peak rarefactional pressures for which IC pulses were observed in the detected data are shown in Fig. 7 as a function of the center frequency and PD. The data show that the peak rarefactional pressure required at rupture threshold increases with increasing frequency and decreases with increasing PD. This peak rarefactional pressure response is consistent with frequency and PD dependencies established in the literature [10]–[12], [16], [30].

## IV. Discussion

We contend that the postexcitation acoustic signal we have identified is a unique signature of IC collapse and a robust indicator of UCA rupture. Although we do not have the capability of high-speed camera imaging, there is substantial circumstantial evidence to support our contention. The most telling feature is that the signal is only present above a certain pressure threshold and that the timing of the signal is such that it occurs after the passage of the acoustic excitation. It has been shown in the shock wave lithotripsy literature (albeit on longer time scales) that this postexcitation acoustic signal is a unique signature of IC collapse [21], [31], [32]. It also has been shown

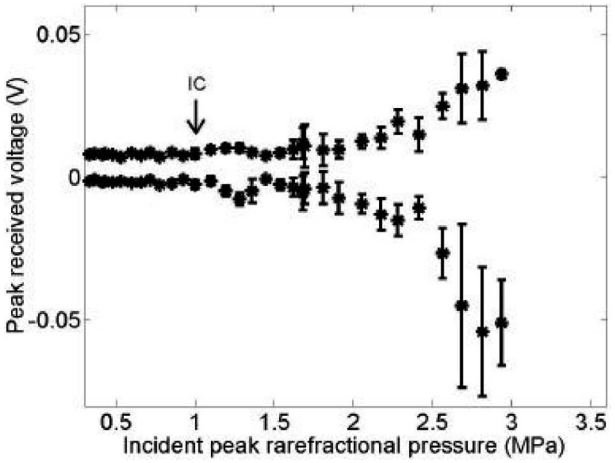


(a)

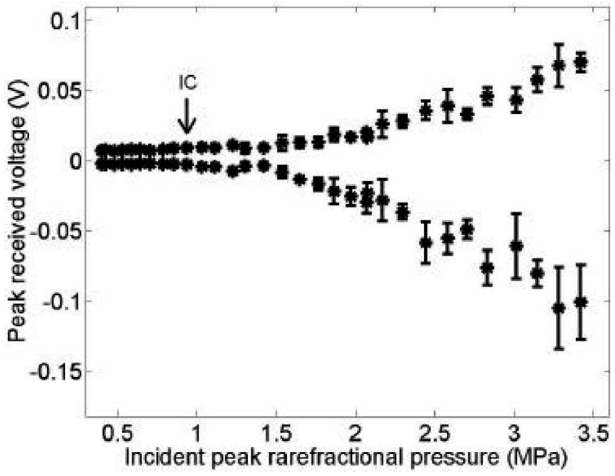


(b)

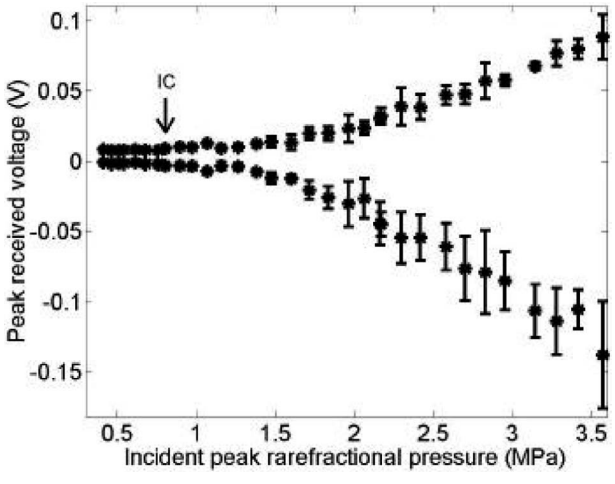


(c)

Fig. 6. Peak positive and negative voltages measured by the 13-MHz PCD receiver as a function of incident peak rarefactional pressure for Optison$^{TM}$ microbubbles excited with a 4.6-MHz pressure waveform. (a) Three-cycle PD. (b) Five-cycle PD. (c) Seven-cycle PD. Error bars show standard deviations. The arrows indicate the incident peak rarefactional pressure thresholds at which the first IC pulse was detected (minimum rupture threshold).

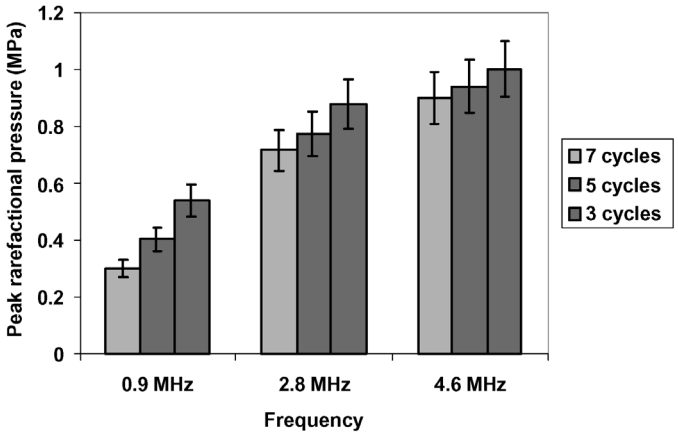


Fig. 7. Minimum rupture thresholds obtained using inertial collapse criterion (error bars represent uncertainties in the hydrophone measurement of the incident peak rarefactional pressure).

with optical observations that microbubble rupture is followed by the creation of unshelled daughter bubbles [12] that then could be nuclei for IC. In another study of the rupture of Optison$^{TM}$ contrast agent, similar postexcitation signals were visible in time-traces from the PCD [33], but no interpretation of these signals was provided by the authors.

We have found observations of signals identified as IC, and rebound responses are consistent with predictions of existing microbubble dynamics models. We modeled the microbubble dynamics using the shell model described by Morgan *et al.* [34]. The model uses the modified Herring equation for microbubble dynamics with two terms augmented to account for the elasticity and viscosity of the shell of the microbubble. The initial microbubble radius used in simulations was 2 $\mu$m and the shell thickness was 15 nm, which correspond to the mean values reported for Optison$^{TM}$ [23]. The shell elasticity was 4 N/m and the shell viscosity was 0.533 Pa.s. The values of these two parameters were taken from the values given by Morgan *et al.* [34]. The measured acoustic waveforms were used as the input acoustic driving pressures to the microbubble dynamics model.

Fig. 8(a) shows the seven-cycle incident pressure waveform measured at the experimentally determined shell rupture threshold of 0.89-MPa peak rarefactional pressure. The modeled microbubble radius as a function of time (r-t curve) is shown in Fig. 8(b), assuming an intact shell. It can be seen that the microbubble only responds when the driving pressure is present, and the oscillations die out as soon as the drive signal stops. The maximum radius attained with this simulation was 3.3 $\mu$m, and we assumed that shell rupture occurred near this radius. In a second simulation, the shell elasticity and viscosity were initially 4 N/m and 0.533 Pa.s; but, once the microbubble radius exceeded 3 $\mu$m, the values for both of these parameters were set to zero so that the effect of the shell was no longer included in the simulation. The resulting r-t curve is shown in Fig. 8(c). In this case, once the shell was removed, the bubble underwent large oscillations that continued well af-

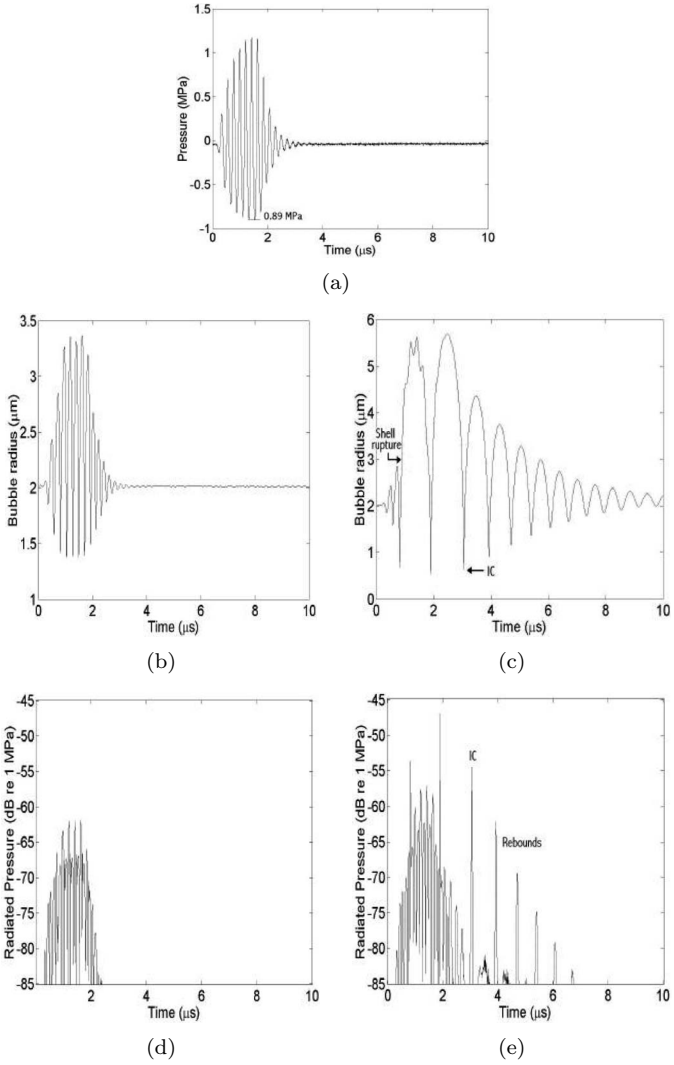


Fig. 8. Bubble dynamics simulations. (a) Measured waveform used as driving pressure. (b) Radius-time curve for a microbubble with an intact shell. (c) Radius-time curve for a microbubble with a shell that ruptures when the radius first exceeds 3 $\mu$m. (d) Radiated pressure from intact bubble (b). (e) Radiated pressure from ruptured bubble (c) with the inertial collapse and rebounds identified.

ter the driving pressure had ceased. In particular, there was an inertial growth and collapse phase that started at 3 $\mu$s and ended at 4 $\mu$s [Fig. 8(c)]. The inertial collapse was followed by many rebounds.

Figs. 8(d) and (e) show the radiated pressure from the simulated microbubbles as a function of time. For the intact shell [Fig. 8(d)], the radiation was only emitted when the driving pulse was present and appeared to be primarily scattering of the driving pulse. The ruptured microbubble [Fig. 8(e)] generated scattering during the excitation, but there also were distinct spikes that could be attributed to strong collapses. These collapses are possible because, once the shell has ruptured, it can no longer act to dampen the response when the driving pressure is present. After the passage of the excitation pulse, the bubble continued to emit a number of distinct spikes due to both the inertial collapse (at 3 $\mu$s) and the subsequent rebounds (e.g., 4 $\mu$s). The simulated pressure waveform of a ruptured bubble [Fig. 8(e)] indicates that the first postexcitation signals identified in PCD traces (e.g., Fig. 5) should correspond to the IC of a ruptured microbubble. The regular temporal separation between postexcitation emissions in the PCD traces is consistent with regularity of IC and free-bubble rebounds in the simulation.

We note that the measured IC time ($t_I$) could be used to estimate the maximum bubble radius of the ruptured contrast agent through application of the Rayleigh collapse model [35] [36]. We define the inertial time $t_I$ as the time from when the microbubble is ruptured during excitation by the negative phase of the ultrasound pulse to its collapse. For example, in Fig. 8(c) $t_I \approx 1$ $\mu$s. The Rayleigh collapse model relates the initial radius of a vapor cavity at rest to the time required by the fluid to collapse the radius to zero. From the predicted r-t curve in Fig. 8(c), we observe that the collapse time—that is, the time from its maximum radius to its collapse—is approximately $t_I/2$. The corresponding maximum bubble radius, predicted using Rayleigh's expression, is:

$$R_{Max} = \frac{t_I}{2} \times \frac{\sqrt{\frac{P_0}{\rho}}}{0.915}, \tag{1}$$

where $P_0$ and $\rho$ are the ambient pressure and density of the liquid, respectively. For water, $R_{Max} \approx 5.5\ t_I$, where $R_{Max}$ is measured in micrometers and $t_I$ in microseconds. For $t_I \approx 1$ $\mu$s in Fig. 8(c), the Rayleigh model predicts a maximum bubble radius of 5.5 $\mu$m. This predicted value corresponds well to the value obtained in the simulation [Fig. 8(b)] (even though the r-t curve is still partially affected by the incident pressure when the maximum radius is reached). By measuring $t_I$, it is possible, therefore, to estimate the maximum size of the unconfined bubble.

Based on identification of the rebound signal, we have experimentally determined minimum shell rupture thresholds (based on peak rarefractional pressure) of Optison™ in terms of frequency (0.9, 2.8, or 4.6 MHz), and PD (three, five, or seven cycles). The minimum thresholds varied from 0.29 to 0.99 MPa. For a 0.9-MHz, seven-cycle incident pulse (PRF 10 Hz), we found the collapse threshold of Optison™ to be 0.29 MPa. This compares favorably with the value of 0.13 MPa for a longer pulse (10 cycles at 1.1 MHz) reported by Chen *et al.* [11], who used broadband noise to identify destruction thresholds. For much longer PDs (in the continuous wave regime), Giesecke and Hynynen [10] estimated peak rarefactional pressure thresholds for Optison™ fragmentation to be 0.4 MPa at 2.18 MHz and 1.6 MPa at 3.3 MHz. Although we only applied a seven-cycle PD as our longest PD, the range of their values encompasses our estimation of 0.71 MPa obtained with an intermediate frequency of 2.8 MHz. Miller and Thomas [30] assessed the IC occurrence based on hydrogen peroxide levels produced during continuous wave ultrasonic exposure of Albunex® and Levovist® (Schering, Berlin, Germany) solutions. Thus, thresholds were determined to be 0.41 MPa at 2.17 MHz and 0.58 MPa at 2.95 MHz (spatial peak pressure amplitude; temporal peaks not reported)

consistent with our thresholds for Optison™. Chomas *et al.* [12] used high-speed photography to measure fragmentation of MP1950 UCA (Mallinckrodt Medical, St. Louis, MO). Although they do not report thresholds, they show that fragmentation occurs at a peak rarefactional pressure of 1.2 MPa for a 2.4-MHz two-cycle pulse indicating that the threshold must be less than 1.2 MPa, which is consistent with our results. Holland *et al.* [18] exposed Albunex® solutions to one-cycle, M-mode and four-cycle Doppler mode clinical ultrasound (at 2.5 MHz and 5.0 MHz). Using a 30-MHz ACD system, they did not detect cavitation for peak rarefactional pressures up to 1.2 MPa. With the exception of the results reported by Holland *et al.* [18], pressure thresholds reported for IC in UCA solutions are in the same general range as pressures estimated for contrast rupture in our study.

We found that the minimum incident peak rarefactional pressure necessary to induce UCA rupture increased with the excitation frequency. For this case in which the studied frequency range was centered above the resonant frequency of the UCA (resonant frequency ≈1 MHz for Optison™ [37]), this result was expected. At lower frequencies the duration of the rarefactional pressure (which drives the microbubble growth) is longer. Longer duration rarefaction should make microbubbles grow to a larger size, and thus be more likely to provoke shell failure. Also, we found that shorter PDs required larger peak rarefactional pressures to induce rupture. This also was expected. Rupture in most materials is a stochastic process. Therefore, by applying more cycles per pulse, shell rupture would be more likely. Similar variations of shell rupture thresholds have been demonstrated as a function of frequency and insonification PD in an experimental contrast agent using a high-speed camera [12] and as a function of PD based on attenuation measurements in Albunex® [16].

## V. Conclusions

This work links postexcitation acoustic emissions detected with a passive cavitation system to inertial collapse and rebounds following rupture of single UCA microbubbles. Minimum incident rarefactional excitation pressure thresholds detected using this signal are consistent with anticipated frequency-dependent and pulse-duration-dependent behavior. Experimental results were consistent with numerical simulations using existing models for microbubble dynamics that considered the process of shell rupture, inertial cavitation, and acoustic emissions. The separation of emissions from the excitation in time and spectral content, the simplicity of measurement equipment, and potential for in vivo application represent significant advantages of this technique compared to techniques previously applied to detect UCA destruction.

## Acknowledgments

This work was supported by the cooperative project for biomedical engineering between the University of Illinois at Urbana-Champaign, and the Centre National de la Recherche Scientifique, France. R. O. C. was supported by a "Bourses de Recherche" from the Scientific Advisory Board of the Mayor of Paris.

## References

[1] A. P. Miller and N. C. Nanda, "Contrast echocardiography: New agents," *Ultrasound Med. Biol.*, vol. 30, pp. 425–434, 2004.

[2] J. Hohmann, T. Albrecht, A. Oldenburg, J. Skrok, and K. J. Wolf, "Liver metastases in cancer: Detection with contrast-enhanced ultrasonography," *Abdom. Imaging*, vol. 29, pp. 669–681, 2004.

[3] J. Eyding, W. Wilkening, M. Reckhardt, G. Schmid, S. Meves, H. Ermert, H. Przuntek, and T. Postert, "Contrast burst depletion imaging (CODIM): A new imaging procedure and analysis method for semiquantitative ultrasonic perfusion imaging," *Stroke*, vol. 34, pp. 77–83, 2003.

[4] K. Wei, A. R. Jayaweera, S. Firoozan, A. Linka, D. M. Skyba, and S. Kaul, "Quantification of myocardial blood flow with ultrasound-induced destruction of microbubbles administered as a constant venous infusion," *Circulation*, vol. 97, pp. 473–483, 1998.

[5] R. V. Shohet, S. Chen, Y. T. Zhou, Z. Wang, R. S. Meidell, R. H. Unger, and P. A. Grayburn, "Echocardiographic destruction of albumin microbubbles directs gene delivery to the myocardium," *Circulation*, vol. 101, pp. 2554–2556, 2000.

[6] J. P. Christiansen, B. A. French, A. L. Klibanov, S. Kaul, and J. R. Lindner, "Targeted tissue transfection with ultrasound destruction of plasmid-bearing cationic microbubbles," *Ultrasound Med. Biol.*, vol. 29, pp. 1759–1767, 2003.

[7] E. Stride and N. Saffari, "On the destruction of microbubble ultrasound contrast agents," *Ultrasound Med. Biol.*, vol. 29, pp. 563–573, 2003.

[8] N. Kamiyama, F. Moriyasu, Y. Mine, and Y. Goto, "Analysis of flash echo from contrast agent for designing optimal ultrasound diagnostic systems," *Ultrasound Med. Biol.*, vol. 25, pp. 411–420, 1999.

[9] C. C. Church and E. L. Carstensen, " 'Stable' inertial cavitation," *Ultrasound Med. Biol.*, vol. 27, pp. 1435–1437, 2001.

[10] T. Giesecke and K. Hynynen, "Ultrasound-mediated cavitation thresholds of liquid perfluorocarbon droplets in vitro," *Ultrasound Med. Biol.*, vol. 29, pp. 1359–1365, 2003.

[11] W. S. Chen, T. J. Matula, A. A. Brayman, and L. A. Crum, "A comparison of the fragmentation thresholds and inertial cavitation doses of different ultrasound contrast agents," *J. Acoust. Soc. Amer.*, vol. 113, pp. 643–651, 2003.

[12] J. E. Chomas, P. Dayton, D. May, and K. Ferrara, "Threshold of fragmentation for ultrasonic contrast agents," *J. Biomed. Opt.*, vol. 6, pp. 141–150, 2001.

[13] J. E. Chomas, P. Dayton, J. Allen, K. Morgan, and K. W. Ferrara, "Mechanisms of contrast agent destruction," *IEEE Trans. Ultrason., Ferroelect., Freq. Contr.*, vol. 48, pp. 232–248, 2001.

[14] R. A. Roy, S. I. Madanshetty, and R. E. Apfel, "An acoustic backscattering technique for the detection of transient cavitation produced by microsecond pulses of ultrasound," *J. Acoust. Soc. Amer.*, vol. 87, pp. 2451–2458, 1990.

[15] S. I. Madanshetty, R. A. Roy, and R. E. Apfel, "Acoustic microcavitation: Its active and passive acoustic detection," *J. Acoust. Soc. Amer.*, vol. 90, pp. 1515–1526, 1991.

[16] P. P. Chang, W. S. Chen, P. D. Mourad, S. L. Poliachik, and L. A. Crum, "Thresholds for inertial cavitation in albunex suspensions under pulsed ultrasound conditions," *IEEE Trans. Ultrason., Ferroelect., Freq. Contr.*, vol. 48, pp. 161–170, 2001.

[17] L. A. Crum, R. A. Roy, M. A. Dinno, C. C. Church, R. E. Apfel, C. K. Holland, and S. I. Madanshetty, "Acoustic cavitation produced by microsecond pulses of ultrasound: A discussion of some selected results," *J. Acoust. Soc. Amer.*, vol. 91, pp. 1113–1119, 1992.

[18] C. K. Holland, R. A. Roy, R. E. Apfel, and L. A. Crum, "In vitro detection of cavitation induced by a diagnostic ultrasound system," *IEEE Trans. Ultrason., Ferroelect., Freq. Contr.*, vol. 39, pp. 95–101, 1992.

[19] W. S. Chen, A. A. Brayman, T. J. Matula, L. A. Crum, and M. W. Miller, "The pulse length-dependence of inertial cavita-

tion dose and hemolysis," *Ultrasound Med. Biol.*, vol. 29, pp. 739–748, 2003.
[20] A. J. Coleman, T. Kodama, M. J. Choi, T. Adams, and J. E. Saunders, "The cavitation threshold of human tissue exposed to 0.2-MHz pulsed ultrasound: Preliminary measurements based on a study of clinical lithotripsy," *Ultrasound Med. Biol.*, vol. 21, pp. 405–417, 1995.
[21] S. L. Ceccio and C. E. Brenne, "Observation of the dynamics and acoustics of travelling bubble cavitation," *J. Fluid Mech.*, vol. 233, pp. 633–660, 1991.
[22] A. Bouakaz, M. Versluis, and N. de Jong, "High-speed optical observations of contrast agent destruction," *Ultrasound Med. Biol.*, vol. 31, pp. 391–399, 2005.
[23] S. Podell, C. Burrascano, M. Gaal, B. Golec, J. Maniquis, and P. Mehlhaff, "Physical and biochemical stability of Optison, an injectable ultrasound contrast agent," *Biotechnol. Appl. Biochem.*, vol. 30, pp. 213–223, 1999.
[24] J. F. Zachary, J. M. Sempsrott, L. A. Frizzell, D. G. Simpson, and W. D. O'Brien, Jr., "Superthreshold behavior and threshold estimation of ultrasound-induced lung hemorrhage in adult mice and rats," *IEEE Trans. Ultrason., Ferroelect., Freq. Contr.*, vol. 48, pp. 581–592, 2001.
[25] R. C. Preston, D. R. Bacon, A. J. Livett, and K. Rajendran, "PVDF membrane hydrophone performance properties and their relevance to the measurement of the acoustic output of medical ultrasound equipment," *J. Phys. E: Sci. Instrum.*, vol. 16, pp. 786–796, 1983.
[26] D. T. Blackstock, M. F. Hamilton, and A. D. Pierce, "Progressive waves in lossless and lossy fluids," in *Nonlinear Acoustics*. M. F. Hamilton and D. T. Blackstock, Eds. Chestnut Hill, MA: Academic, 1998, pp. 65–150.
[27] K. Raum and W. D. O'Brien, Jr., "Pulse-echo field distribution measurements technique for high-frequency ultrasound sources," *IEEE Trans. Ultrason., Ferroelect., Freq. Contr.*, vol. 44, pp. 810–815, 1997.
[28] M. Postema, A. van Wamel, C. T. Lancee, and N. de Jong, "Ultrasound-induced encapsulated microbubble phenomena," *Ultrasound Med. Biol.*, vol. 30, pp. 827–840, 2004.
[29] M. Postema, P. Marmottant, C. T. Lancee, S. Hilgenfeldt, and N. de Jong, "Ultrasound-induced microbubble coalescence," *Ultrasound Med. Biol.*, vol. 30, pp. 1337–1344, 2004.
[30] D. L. Miller and R. M. Thomas, "Ultrasound contrast agents nucleate inertial cavitation in vitro," *Ultrasound Med. Biol.*, vol. 21, pp. 1059–1065, 1995.
[31] A. J. Coleman, M. J. Choi, J. E. Saunders, and T. G. Leighton, "Acoustic emission and sonoluminescence due to cavitation at the beam focus of an electrohydraulic shock wave lithotripter," *Ultrasound Med. Biol.*, vol. 18, pp. 267–281, 1992.
[32] R. O. Cleveland, O. A. Sapozhnikov, M. R. Bailey, and L. A. Crum, "A dual passive cavitation detector for localized detection of lithotripsy-induced cavitation in vitro," *J. Acoust. Soc. Amer.*, vol. 107, pp. 1745–1758, 2000.
[33] W. S. Chen, T. J. Matula, and L. A. Crum, "Ultrasound contrast agent behaviour near the fragmentation threshold," in *Proc. IEEE Ultrason. Symp.*, 2000, pp. 1935–1938.
[34] K. E. Morgan, J. S. Allen, P. A. Dayton, J. E. Chomas, A. L. Klibanov, and K. W. Ferrara, "Experimental and theoretical evaluation of microbubble behavior: Effect of transmitted phase and bubble size," *IEEE Trans. Ultrason., Ferroelect., Freq. Contr.*, vol. 47, pp. 1494–1509, 2000.
[35] C. C. Church, "A theoretical study of cavitation generated by an extracorporeal shock wave lithotripter," *J. Acoust. Soc. Amer.*, vol. 86, pp. 215–227, 1989.
[36] T. G. Leighton, "Cavitation inception and fluid dynamics," in *The Acoustic Bubble*. San Diego, CA: Academic, 1994, pp. 67–128.
[37] P. D. Krishna and V. L. Newhouse, "Second harmonic characteristics of the ultrasound contrast agents Albunex® and FSO69," *Ultrasound Med. Biol.*, vol. 23, pp. 453–459, 1997.

**Azzdine Y. Ammi** is currently a Ph.D. student in Acoustical Physics, at the University Pierre et Marie Curie, Paris VI, France. His dissertation is on detection and modeling of ultrasound contrast agent shell rupture. He received his Master of Science in Acoustical Physics, in 2002, from the University Denis Diderot, Paris VII, France. He received his Bachelor of Science in Applied Physics, in 2001 from the University Denis Diderot, Paris VII, France, which included an academic year (third) at the University of York, England (European ERASMUS Program).

**Robin O. Cleveland** received his B.Sc. and M.Sc. in Physics from The University of Auckland, Auckland, New Zealand in 1989 and 1991, respectively. He received a Ph.D. in Mechanical Engineering from the University of Texas at Austin, Austin, TX, in 1995. After completing his Ph.D. studies he was awarded the F. V. Hunt post-doctoral fellowship of the Acoustical Society of America which was carried out at the University of Washington at Seattle, Seattle, WA. He joined the faculty of Boston University, Boston, MA, in 1997 where he is currently an Associate Professor of Aerospace and Mechanical Engineering. Dr. Cleveland's research interest is in the propagation of nonlinear sound in complex media and recent projects include: shock wave lithotripsy, therapeutic ultrasound, and harmonic imaging in diagnostic ultrasound. He is a member of the American Society of Mechanical Engineers and a Fellow of the Acoustical Society of America.

**Jonathan Mamou** was born in Saint-Germain-En-Laye, France in 1978. In July 2000, he graduated from the Ecole Nationale Supérieure des Télécommunications in Paris, France. In January 2001, he began his graduate studies in electrical and computer engineering at the University of Illinois at Urbana-Champaign, Urbana, IL. He received his M.S. and Ph.D. degrees in May 2002 and 2005, respectively. He is now a member of the research staff at the Riverside Research Institute in New York, NY. His fields of interest include theoretical aspects of ultrasonic scattering, ultrasonic medical imaging, and biomedical image processing. Jonathan Mamou is a member of IEEE, the American Institute of Ultrasound in Medicine, and the Acoustical Society of America.

**Grace Wang** was born in Downers Grove, IL, in 1984. She is currently pursuing her B.S. degree in electrical engineering at the University of Illinois in Urbana-Champaign, Urbana, IL, and has been recognized with numerous departmental awards. Her research interests include modeling of shelled contrast agents.

**S. Lori Bridal** (S'93–M'95) was born in Oklahoma City, OK, in 1967. She received the B.S. degree in physics from Oklahoma State University in Stillwater, OK, in 1988 and the M.A. and Ph.D. degrees in physics from Washington University, St. Louis, MO, in 1990 and 1994, respectively. In 1995, she was awarded a Chateaubriand Fellowship by the French government for post-doctoral studies in the Laboratoire d'Imagerie Paramétrique (L.I.P.) at the University Pierre et Marie Curie in Paris, France. Awarded the CNRS (French National Center of Scientific Research) bronze medal in 2004. Currently she is a CNRS research scientist and continues research at the L.I.P. on topics including quantitative characterization and imaging of biological materials. General research interests include high frequency ultrasound, tissue characterization and ultrasound contrast agents.

**William D. O'Brien, Jr.** (S'64–M'70–SM'79–F'89) received the B.S., M.S., and Ph.D. degrees in 1966, 1968, and 1970, from the University of Illinois, Urbana-Champaign, Urbana, IL.

From 1971 to 1975 he worked with the Bureau of Radiological Health (currently the Center for Devices and Radiological Health) of the U.S. Food and Drug Administration. Since 1975, he has been at the University of Illinois, where he is the Donald Biggar Willet Professor of Engineering. He also is Professor of Electrical and Computer Engineering and of Bioengineering, College of Engineering; Professor of Bioengineering, College of Medicine; Professor of Nutritional Sciences, College of Agricultural, Consumer and Environmental Sciences; Research Professor in the Beckman Institute for Advanced Science and Technology; and Research Professor in the Coordinated Science Laboratory. He is the Director of the Bioacoustics Research Laboratory. His research interests involve the many areas of ultrasound-tissue interaction, including biological effects and quantitative ultrasound imaging for which he has published 299 papers.

Dr. O'Brien is a Fellow of the Institute of Electrical and Electronics Engineers, the Acoustical Society of America and the American Institute of Ultrasound in Medicine, and is a Founding Fellow of the American Institute of Medical and Biological Engineering. He was recipient of the IEEE Centennial Medal (1984), the AIUM Presidential Recognition Awards (1985 and 1992), the AIUM/WFUMB Pioneer Award (1988), the IEEE Outstanding Student Branch Counselor Award for Region 4 (1989), the AIUM Joseph H. Holmes Basic Science Pioneer Award (1993), and the IEEE Ultrasonics, Ferroelectrics, and Frequency Control Society Distinguished Lecturer (1997–1998). He received the IEEE Ultrasonics, Ferroelectrics, and Frequency Control Society's Achievement Award for 1998 and Distinguished Service Award for 2003, and the IEEE Millennium Medal in 2000. He has served as Co-Chair of the 1981, 2001 and 2003 IEEE Ultrasonic Symposia, and General Chair of the 1988 IEEE Ultrasonics Symposium. He has served as President (1982–1983) of the IEEE Sonics and Ultrasonics Group (currently the IEEE Ultrasonics, Ferroelectrics, and Frequency Control Society), Editor-in-Chief (1984–2001) of the *IEEE Transactions on Ultrasonics, Ferroelectrics, and Frequency Control*, President (1988–1991) of the American Institute of Ultrasound in Medicine and Treasurer (1991–1994) of the World Federation for Ultrasound in Medicine and Biology, and on the Board of Directors (1988–1993) of the American Registry of Diagnostic Medical Sonographers.